Characterization of a self-assembled monolayer of O-(2-Mercaptoethyl)-O′-methyl-hexa(ethylene glycol) (EG7-SAM) on gold electrodes.

Miriam Chávez, Guadalupe Sánchez-Obrero, Rafael Madueño, José Manuel Sevilla, Manuel Blázquez, Teresa Pineda*

Department of Physical Chemistry and Applied Thermodynamics, Institute of Fine Chemistry and Nanochemistry, University of Cordoba, Campus Rabanales, Ed. Marie Curie 2ª Planta, E-14014 Córdoba, Spain

AUTHOR EMAIL ADDRESS tpineda@uco.es

AUTHOR ORCID Nº: 0000-0002-1504-903X

Phone number: +34-957-218646

Fax number: +34-957-218618

Abstract

The modification of surfaces by polyethylene glycol (EGn) is an approach used to reduce the antifouling effects of these materials in a biological medium. It has been found that the packing density and conformational order of these molecules in the films are crucial for the inhibition of unspecific protein adsorption. In this work, we present a study of the formation and characterization of a self-assembled monolayer of O-(2-Mercaptoethyl)-O′-methyl-hexa(ethylene glycol) (EG7-SAM) on either poly-oriented or Au(111) single crystal surfaces. The final properties of the formed EG7-SAMs are studied by examining the reductive desorption process as well as the electronic and ionic blocking behavior of these layers, under different experimental conditions, by using cyclic voltammetry and electrochemical impedance spectroscopy. Additional information of the structure, composition and organization is obtained by absorption-reflection infrared and X ray photoelectron spectroscopies and contact angle measurements. In contrast to the behavior observed with alkanethiols, the EG7-SAM shows the best final organization at a modification time of 1h. The antifouling properties of this EG7-SAM against the adsorption of the bovine serum albumin protein in a phosphate saline medium, has been evidenced by using the electrochemical quartz crystal microbalance technique.

Keywords. Polyethylene glycol, self-assembled monolayer, gold, cyclic voltammetry, electrochemical impedance spectroscopy, infrared spectroscopy, X ray photoelectronic spectroscopy, contact angle measurements, electrochemical quartz crystal microbalance.

1. Introduction

The covalent attachment of poly(ethylene glycol) chains (PEG or EGn, being n the number of EG units) to bioactive substances has been long defined as PEGylation [1] and recently, it has been applied to the modification of nanoparticle surfaces for its use in different fields to induce, on one hand, aqueous solubility, and on the other, to sterically shield nanoparticle surfaces to effectively minimize opsonisation and prolong blood circulation time *in vivo* [2, 3]. Although these applications are based in the ability of avoiding protein unspecific adsorption, the factors that influence the interactions and circulation of PEGylated nanoparticles in the biological fluids are numerous and many efforts have been devoted to rationalized them. Molecular weight, surface density and conformation of the PEG chains are the most studied parameters and there is no doubt that is the precise knowledge of how they impact on the systemic administration that will lead to more efficacious products [3-5]. Complementary structural studies of these EG polymer layers on flat surfaces may help in understanding the suppressive effect for protein unspecific adsorption and in the translation to these drug delivery systems to the living systems [6, 7].

Self-assembled monolayers (SAMs) of oligo(ethylene glycol) (OEG)-terminated alkanethiols on gold and silver substrates have been widely used to analyse the factors that influence the minimization of protein resistance [8-11] and within the facts responsible for this undesirable phenomenon, steric repulsion, large exclusion volume, rapid mobility of highly hydrated chains, low EG-water interfacial energy and weak interactions with the proteins have been mentioned. Earlier studies [8, 12, 13] comparing SAMs with short terminal EG segments to that of PEG, focussed on the steric repulsion model that attributes the protein resistance to the balance between this steric repulsion and the attractive forces. The steric repulsion has an elastic component caused by the compression and restriction of the EG segments and an osmotic component due to the loss of water by both the chains and the proteins. As the SAMs with the shorter EG terminal fragments have a more compact structure, the protein resistance was generally attributed to the osmotic component of the steric repulsion model. However, Grunze et al. [10, 14] suggest that protein resistance of EG terminated SAMs is a consequence of the stability of the interfacial water layer, which prevent direct contact between the surface and the protein. Moreover, the conformation of the terminal strand contributes to the ability to bind water, being the helical but not the all-trans conformation the one which

behaves as amphiphilic with respect to water, increasing the hydrogen bond density, and thus preventing irreversible protein adsorption.

SAMs formed with molecules containing an EG strand closer to the substrate binding and an alkane terminal portion have been used as models for hybrid bilayer membranes to allow for water and/or protein fragments incorporation. Although this hydrophilic spacer should retain a linear framework and provide a good coverage due to the nearly perfect match between the cross-sectional area of the structures, a less ordered conformation than the alkanethiol portion is expected based on the presence of ether oxygen atoms in the skeleton. However, infrared and ellipsometry data suggest a lamellar-type crystal morphology in an ordered 7/2 helical structure oriented normal to the substrate independently of the length of the alkyl group [15, 16]. These results make the authors to expect that the EG strands itself can form conformationally well-defined, helical SAMs and studied the conformation and the resistance to protein adsorption of chains that contain only EG units [17, 18]. EG6-SAMs assembled on gold from 95 % ethanol solutions show well-ordered 7/2 helical conformation, similar to that of the folded chain crystal polymorph of PEG, and a behaviour that approaches to a near ideal capacitor but, when assembled from other solvents, the structure was found more variable and less ordered [18, 19]. The EGn-SAMs structures vary with n, being helically ordered for n > 4, as seen by infrared spectroscopy and electrochemical impedance spectroscopy data, whereas with less than 6 EG units in the chain, the films are rapidly penetrated by water [16, 18, 20, 21].

The use of EGn films for the development of electrochemical biosensors requires that its interfacial structure allows electron transfer between the electrode and the redox species in solution. There have been many studies in the literature dealing with EGn films of various thickness attached to different electrode surfaces that uses the extent of passivation or permeation of redox pairs to draw information about the film structure and properties [22-24]. These studies focus on the sieving effect of the films as they allow the permeation of the molecules depending on molecular size [22] or the solubility of the redox probes into the film [23, 24]. The attachment of thiolated EGn molecules of definite length on gold electrodes can serve as platform to better study these phenomena. In this sense, the studies of Doneux et al. [25, 26] using an EG7-SAM on gold and applying electrochemical techniques showed that the film consists of a compact and fairly hydrated single monolayer with a peculiar behaviour that they explain on the basis of the hydration properties of the monolayer as well as the $[Fe(CN)_6]^{3-/4-}$ couple.

In the present work, the formation and characterization of a SAM of EG7 on either poly-oriented or single crystal gold electrodes and its behaviour against the unspecific adsorption of proteins employing different experimental techniques are performed. Reductive desorption (RD) processes of the SAMs under different experimental conditions inform about their structural organization and compactness and the studies of the electronic and ionic blocking properties performed by using electrochemical techniques such as cyclic voltammetry (CV) and electrochemical impedance spectroscopy (EIS) in the presence and absence of redox probes, complete this information. More insight on the film's properties are obtained by infrared and XPS spectroscopies and contact angle measurements. Finally, the possible adsorption of proteins in the EG7-SAM is checked by electrochemical quartz crystal microbalance.

2. Experimental section.

2.1. Chemicals.

O-(2-Mercaptoethyl)-O′-methyl-hexa(ethylene glycol) (EG7), Potassium hexaferri-cyanide and potassium hexaferrocyanide ($[Fe(CN)_6]^{3-/4-}$), ferrocenemethanol and hexaammineruthenium chloride were purchased from Aldrich-Sigma (purity ≥ 99%). The rest of the reagents were from Merck analytical grade. All solutions were prepared with deionized ultrapure water produced by Millipore system.

2.2. Experimental Methods.

Electrochemical experiments were performed on an Autolab (Ecochemie model Pgstat30) instrument attached to a PC with proper software (GPES and FRA) for the total control of the experiments and data acquisition. A conventional three electrode cell comprising a platinum coil as counter electrode, a 50 mM KCl calomel (CE 50mM) as reference electrode and either a poly-oriented (po-Au) or a single crystal (111) gold (Au(111)), as the working electrodes, was used. The po-Au electrode was a homemade sphere obtained by melting a gold wire up to reach a diameter of approximately 2 mm and attached to the gold wire that serves as electrode connection. The Au(111) single crystal was from Arrandee™ (based on a 250 nm thick Au layer adhered to a 2.5 nm thin chromium layer deposited on a Borosilicate glass 11 x 11 mm flat surface). Before each experiment, the working electrodes were annealed in a natural gas flame to a light-red melt, cooling in air and then transferred to the electrochemical cell or to the working solutions. The state of the surface conditions was confirmed by cyclic voltammogram shapes taken in 0.01M

$HClO_4$. This surface treatment was the most appropriate for producing a surface that was clean, ordered, and reproducible. The real area of the gold electrodes was determined from the charge involved in the gold oxide reduction peak obtained under these conditions (A(po-Au) = 0.24 cm^2).

Electrochemical impedance experiments were recorded in aqueous solutions of KNO_3 0.1 M in the absence and presence of 1 mM $[Fe(CN)_6]^{3-/4-}$. The later were obtained at the midpoint potential of the CV for the naked electrode, at 0.08 V. The spectra in the absence of the redox couple were recorded at different potentials. The frequency range used in all experiments was from 100 kHz to 0.1 Hz and the pulse amplitude was of 10 mV.

The electrochemical quartz crystal microbalance used was a CHI 400c series. The quartz crystals were covered by a layer of Ti of 100 Å and a layer of polished gold of 1000 Å. These crystals operate at 8 MHz. The mass deposited is obtained by using the Sauerbrey equation by using a calibration constant of 1.4 ng/Hz [27].

Infrared-reflection absorption spectroscopy (IRRAS) was measured by using a JASCO 6300 FTIR single (He-Ne) laser beam spectrometer in the 400-4000 cm^{-1} wavenumber range, at a resolution of 4 cm^{-1}. Spectra Manager software was employed for data collection and analysis. A Pike Technologies-VeeMAX^{TM}, variable angle specular reflectance accessory was used. Before measurements, the interferometer and sample compartment were purged with a flux of dry air of 8 l/min for half an hour. This flux was supplied by a compressed air adsorption dryer (K-MT LAB, Parker/Zandet GmbH&Co.KG). To record IRRAS spectra, Au-modified substrates were placed on a mask platform with an aperture of 10 mm in diameter to define the position and sampling dimensions where the beam spot was collimated. A p-polarized laser beam at a grazing angle of 80° was selected to interact with the sample surface for enhancement of the IR signals collected by the instrument MCT-detector.

XPS analysis was performed using an MCD SPECS Phoibos 150 spectrometer (from the Servicio Central de Apoyo a la Investigación (SCAI) of the Universidad de Cordoba) employing non-monochromatized (12 kV, 300 W) Mg Kα radiation (1253.6 eV). The substrate, either clean or modified, was mounted on a steel sample holder and transferred to the XPS analytical chamber. The working pressure was less than $5 \cdot 10^{-9}$ Pa. The spectra were collected using a take-off angle of 45° respect to the sample surface plane. The spectrometer was calibrated by the binding energy (BE) of the Au $4f_{7/2}$ line at 84.0 eV. The standard deviation for the BE values was 0.2 eV. Survey scans were run in the 0-1100 eV range (pass energy 60 eV), and higher resolution scans were recorded for the C

1s, O 1s and S 2p regions. The analysis involved Shirley background subtraction, and whenever necessary, spectral deconvolution was carried out by nonlinear least-squares curve fitting adopting a Gaussian sum function, employing the software CASA-XPS.

Contact Angle (CA) Measurements were conducted by using an Optical Tensiometer Theta T200 device (Attension, Biolin Scientific) equipped with a high-speed camera (420 fps). The CA of the formed SAMs were measured in sessile drop method. The experiments were performed at room temperature and at open atmosphere. The results are given as an average of six measurements.

2.3. Formation of the EG7-SAM.

The SAMs were formed by contacting the gold substrates with 1.0 mM EG7 ethanol solutions for the desired modification time. After the immersion time, the modified electrode was thoroughly washed with ethanol and water and then drying under a nitrogen stream. The po-Au electrode was used in all the electrochemical experiments, unless otherwise stated and the Au(111) single crystal for IRRAS, XPS and CA measurements.

3. Results and discussion

3.1. Electrochemical characterization of the EG7-SAMs formed at different immersion times.

The reductive desorption (RD) process monitored by cyclic voltammetry (CV) has long been used to inform about properties related to film stability and compactness, as well as to the suitability for the SAM preparation methods. We carried out preliminary experiments involving the evaluation of the influence of modification time in the SAMs properties. Figure 1 shows a set of CVs recorded with the freshly prepared EG7-SAMs in the potential range from −0.50 to −1.30 V, in KOH 0.1 M solutions. The EG7-SAM-Au substrates are removed from the formation solution (1 mM EG7 in ethanol), and subsequently washed and immersed in the working solution under potential controlled conditions (at -0.5 V). When the current density at this potential becomes constant, the CVs are recorded. As a general behaviour, all the curves present a well visible although small peak (peak I) at higher potentials, and a last very intense peak (peak III) at lower potentials, that show some kind of fine structure that also changes with modification time (peak IV). Moreover, a small signal between these peaks (peak II) is observed. The peak potentials do not significantly vary at modification times lower than 1 h (Figure 1 b). At larger modification times the lower resolution of these peaks does not allow to draw a clear conclusion about its nature and will not be further commented.

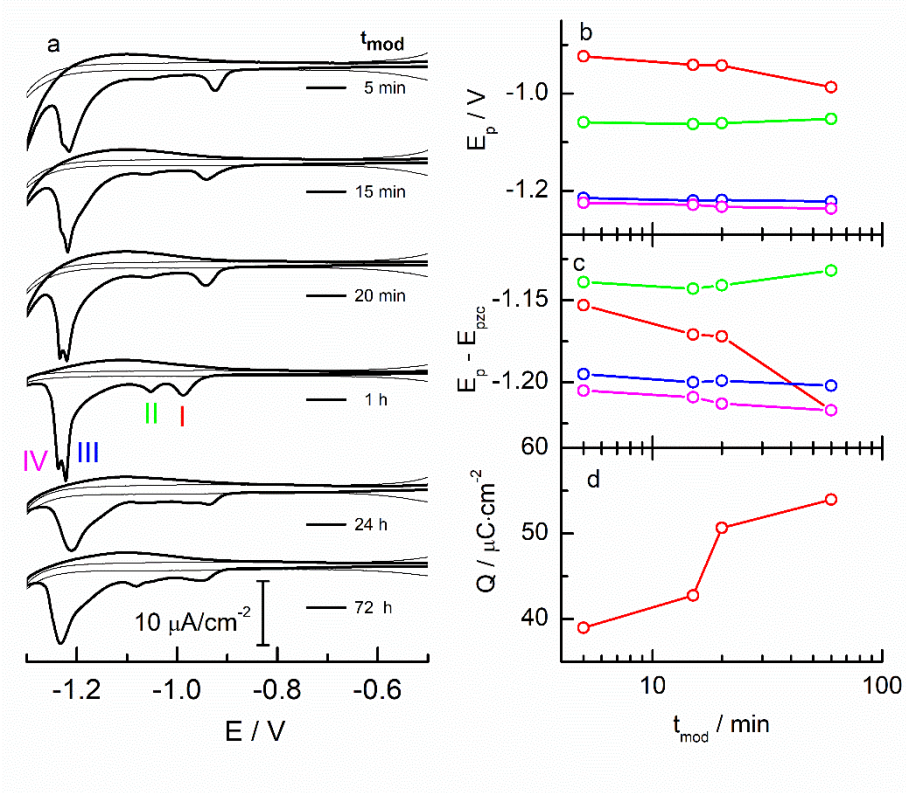

Figure 1. (a) CVs for the RD process of the EG7-SAM-po-Au formed at different modification times. The CVs are obtained in KOH 0.1 M; scan rate: 0.02 V/s (the thick and thin lines in each case correspond to the EG7-SAM and naked electrode, respectively); Plots of (b) peak potentials, E_p, (c) $E_p - E_{pzc}$ and (d) the overall charge densities of the RD peaks as a function of modification time.

The presence of well-defined peaks in the CVs for the RD process obtained at po-Au electrodes has been related to the breakage of the S-Au bond from gold facets of different crystalline orientations, from which at least the low-index facets Au(111), (100) and (110) have been clearly identified in SAMs formed at po-Au electrodes [28-32]. The direct relationship of the desorption potentials with the *pzc* for the different facets of the naked electrode would mean that the process is only governed by the interfacial electric field. However, the values of E_p-E_{pzc} are found to vary for the different facets and SAMs chemical composition being the existence of lateral attractive forces one of the main factors that affect this discrepancy. These lateral interactions also depend on the surface structure, including not only the type of facet but also the surface roughness [32]. Moreover, multiwave responses in RD processes carried out in smooth surfaces have been interpreted as the existence of domains of different sizes that desorb at different potentials

due to variation in cohesive interactions between chains as well as in permeability to counterions and solvent [33].

We have plotted E_p-E_{pzc} values at the different modification times for all the peaks obtained (Figure 1c) and the results show that all the peaks get closer in an interval of ~~50~~ 60 mV (E_{pzc} values applied are +0.23, +0.08 and -0.02 V for (111), (100) and (110) facets of gold, respectively, that correspond to values measured in 10 mM $HClO_4$ [32, 34]). However, it is well known that the presence of the SAM on the electrode surface leads to large shifts on the E_{pzc} that depend on the surface coverage, the adsorption/desorption of ions and the surface dipole of the monolayer [35]. In the present analysis, the only object to subtract E_{pzc} values to the peak potentials is to see if these normalized values are only influenced for the gold facet where they were grown up or, on the contrary, there is additional phenomena playing a role in the occurrence of the peaks [36]. These results would indicate that peaks I and III/IV correspond to domains of molecules desorbed from the (111) and (110) facets, respectively, and that the fine structure observed (peaks III/IV) should be ascribed to the existence of domains with different lateral interactions. .

We have checked the surface recognition phenomenon by building an EG7-SAM on an Au(111) single crystal electrode and the results are plotted in Figure 2. As it can be observed, the unique peak shown at the Au(111) electrode at -0.99 V, coincides in potential with the peak I for the RD obtained at the po-Au electrode, confirming our hypothesis. Thus, influences of lateral interactions in the RD potential values for the molecules in these domains cannot be discarded

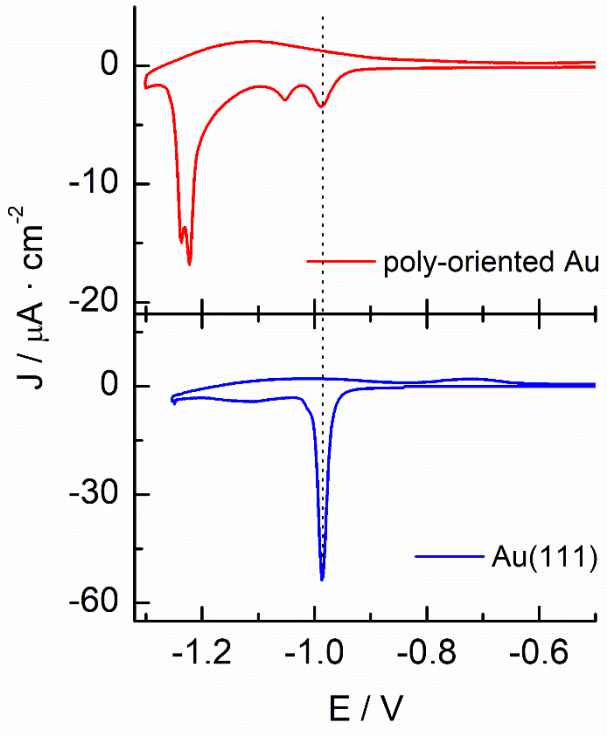

Figure 2. CVs for the RD process of the EG7-SAM formed in two different gold substrates at a modification time of 1 h, in KOH 0.1 M. Scan rate: 0.02 V/s.

The information on SAMs surface coverage based on RD processes is based in the widely accepted reaction [36-38],

$$R\text{-}S\text{-}Au + solvent + 1e^- \longrightarrow Au_{solv} + R\text{-}S^-_{solv} \qquad (1)$$

where Au_{solv} and $R\text{-}S^-_{solv}$ stand for the solvated thiolate and gold surface, respectively. This equation is a solvent substitution reaction that gives a chemical description of the initial and final states of the process and takes into account the energetic contributions involved in SAMs RD such as substrate-adsorbate, SAM-solvent, lateral interactions, substrate-solvent and surfactant solvation [32, 36]. In this sense, the charge density, Q, should contain not only the faradaic charge due to the RD but also the double layer charging contribution. Moreover, it has been pointed out that although we use the reaction (1) to account for the RD process, the charge flowing to the interface per desorbed molecule is not an integer equal to the number of electron transferred from metal to the molecule but, this value depends on electrode potential and the nature of the supporting electrolyte [39]. Thus, as an approximate tool, we measure the charge involved in the RD CVs of Figure 1 and the results are shown in Figure 1d. The charge densities obtained increase with modification time up to 1h and then, remain constant. Independent of the absolute values obtained, it can be said that the EG7 formed at shorter times should

correspond to a sub-monolayer while at higher times, a saturated coverage is obtained. It is interesting to note that in the time interval of 20 to 60 min the EG7-SAM suffers a reductive process with well resolved peaks that loose resolution upon increasing modification time. If we accept that the presence of resolved peaks is related with the presence of domains with a preferential organization, it can be concluded that when the modification time is of 1h, the monolayer have reached the maximum charge density, that is, its maximum coverage, and the higher organization in domains. A roughly calculation of the surface coverage Γ, by taking into account the charge density obtained under this condition, gives us a value of 5.7×10^{-10} mol·cm^{-2} and an area per EG7 molecule of 29 ± 1 Å^2. A cross sectional area of 21.38 Å^2/EG chain has been determined based on the X-ray unit cell dimensions of the crystalline polymer, and is presumed to be achieved for the alkylated EGn SAMs where the EG strands acquire the helical conformation [15], is not observed in the present system. This larger fingerprint of the EG7 molecules must be due to a lower compactness of the layer, probably due to the existence of a larger conformational freedom in the absence of alkyl chains in the molecules.

To get more insight into the properties, the following potential programs were applied to the EG7-SAM. First, the modified electrode is contacted with the alkaline solution at the initial potential (-0.4 V) and the scan to negative direction is initiated up to values where the complete monolayer is reductively desorbed. Then, the potential is scanned to positive values including the gold surface oxidation region and ended after scanning to negative values to the initial potential (Figure 3). Comparing to the blank profile, the EG7-SAM modified electrode shows, besides the RD peaks already commented, a small current density broad peak in the anodic frame (at -1.135 V) that could be ascribed to a partial re-adsorption of the desorbed EG7 molecules in the cathodic scan probably giving place to a sub-monolayer coverage that, however, does not affect in great extension the oxidation of the gold surface as the anodic peak at higher potentials almost coincides with that of the clean electrode. Second, the freshly modified electrode is now submitted to a potential scan in the positive direction to investigate if the presence of the EG7-SAM passivates the gold surface against oxidation. In fact, the CV shows that the onset for surface oxidation is displaced more than 250 mV in the presence of the monolayer (blue double arrow in the CV). At around 0.275 V, a burst of oxidation current is observed that should correspond to the oxidative desorption of the monolayer concomitant with the oxidation of the gold surface. In the reverse scan, when the potential reaches the values for the RD,

a small signal coinciding with the lowest potential peak obtained for the direct RD process is observed.

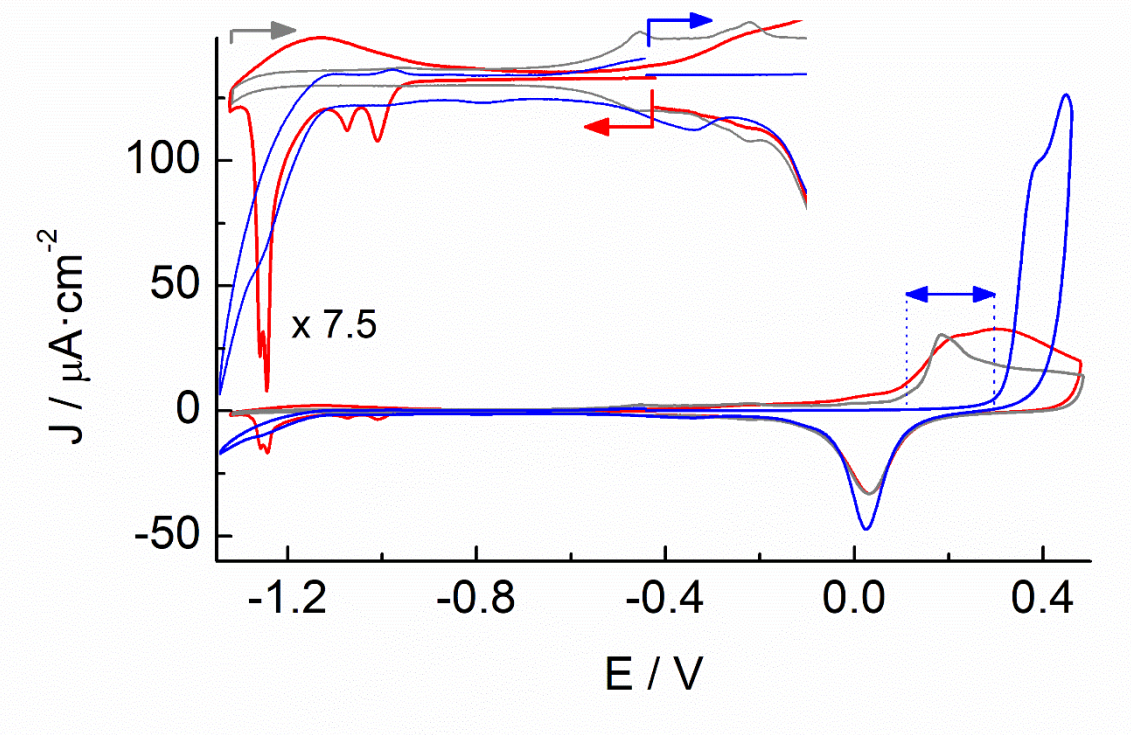

Figure 3. CVs for the reductive (red line) and oxidative (blue line) desorption processes of the EG7-SAM-Au, formed at a modification time of 1 hour. KOH 0.1 M, scan rate: 0.02 V/s. The grey curve represents the electrochemical profile for the naked gold electrode in the same medium. The inset shows an expanded view (in the Y axis direction) of the double layer region for the three curves showing coloured arrows to signal the direction of the scans and the trends of the current densities obtained.

3.2. Blocking behaviour of EG7-SAM.

The EG7-SAM can be further characterized by analysing the effect on the heterogeneous electron transfer rate of some redox couples such as $[Fe(CN)_6]^{3-/4-}$, $[Ru(NH_3)_6]^{3+/2+}$, $Fc(MeOH)_2^{0/+}$. Whereas the CVs for $[Ru(NH_3)_6]^{3+/2+}$ and $Fc(MeOH)_2^{0/+}$ redox probes are insensitive to the presence of the molecular layer (data not shown), that of $[Fe(CN)_6]^{3-/4-}$ shows important changes when compared to the naked electrode (Figure 4a). It can be observed that the electrochemical signal is completely suppressed when the EG7-SAM is present. Only a very small current density can be measured (see expanded view of the CVs in the insert) as it is typical for good blocking behaviour. However, the inhibition seems to be slightly weaker at immersion times higher than 1 h. The impedance data (Figure 4b) show the same trend, with a decrease in the diameter of the semicircle as the

modification time increases. Under these experimental conditions, only the semicircle is seen, whereas the linear portion of the impedance spectrum is absent, indicating absence of diffusion.

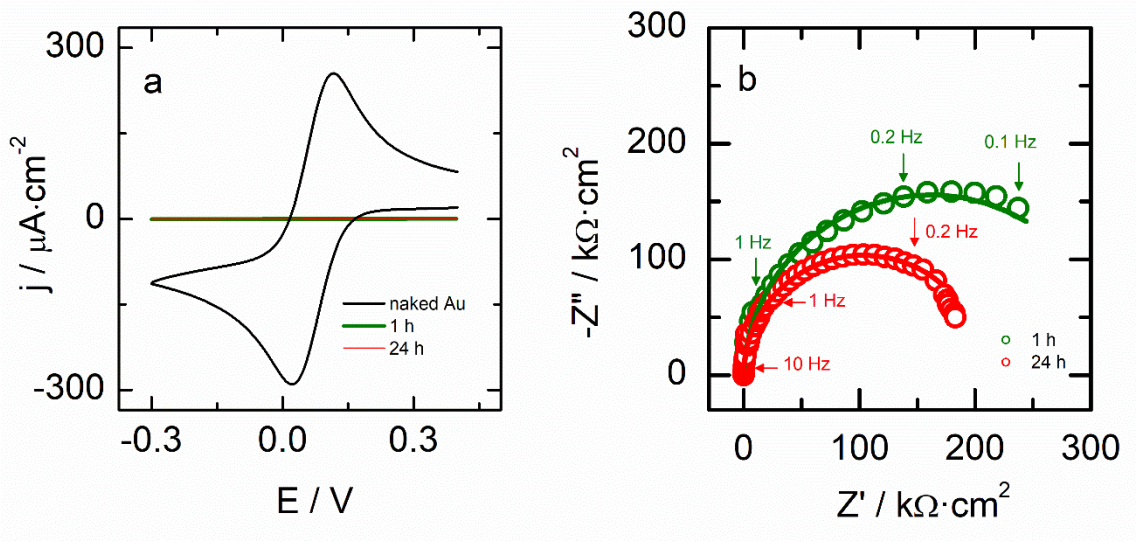

Figure 4. (a) CVs and (b) impedance spectra of 1 mM $[Fe(CN)_6]^{3-/4-}$ in KNO_3 0.1 M in a naked and EG7-SAM po-Au electrode at different times of modification; scan rate for CVs is 0.1 V/s; the impedance spectra are recorded at the midpoint of the CV: 0.08 V. Some frequency values are indicated. Green and red open circles represent the experimental data and solid green and red lines are the best fits obtained by using a simplified Randles equivalent circuit, for the impedance spectra recorded for the EG7-SAM prepared at 1 and 24 h modification time, respectively.

Recently, Whitesides et al. [40] have examined the phenomenon of charge transport by tunnelling across SAMs of EGn of different chain lengths and have found that the attenuation factor β across these SAMs is much lower ($\beta(EGn) = 0.29 \pm 0.02 \cdot n_{atom}^{-1}$) than the observed with alkanethiolates. If the exponential decrease with the chain length of the EG7 chain, with a tunnelling factor of β = 0.29 per atom unit in the chain, d, is taken into account (equation 2), the apparent electron transfer rate constant, k_{ap}, obtained would be of around $6.5 \cdot 10^{-5}$ cm·s^{-1} for a tunnelling transport mechanism by using a k_o value of 0.033 cm/s [41].

$$k_{ap} = k_o.e^{-\beta \cdot d} \qquad (2)$$

The impedance spectra have been fitted by using a simplified Randles circuit (without Warburg element, as the spectra do not show diffusion features) and the charge transfer

resistances have been obtained. From these data, k_{ap} values can be obtained by using equation (3):

$$k_{ap} = \frac{RT}{n^{2} \cdot F^{2} \cdot R_{ct} \cdot A \cdot c} \qquad (3)$$

where R is the gas constant, T the temperature, F the Faraday constant, n the number of electrons, A the geometric area of the electrode and c the concentration of the redox pair. The k_{ap} values obtained for the EG7-SAMs formed at 1 and 24h modification time, are $4.4 \cdot 10^{-7}$ and $6.4 \cdot 10^{-7}$ cm·s^{-1}, respectively, that are much lower than the above given value based on the tunnelling mechanism. Although the occurrence of such a mechanism cannot be discarded under these conditions, an additional concomitant effect must take place that produces this strong blockage of the ferricyanide redox probe by the EG7-SAM. This behaviour has already been described for this system by Doneux et al. [25, 26], that investigated the heterogeneous electron transfer processes of different redox probes either positive, neutral, or negatively charged, across EG7-SAMs built on a polycrystalline gold electrode. They found that, as we also report in the present work, only the ferricyanide redox probe is affected, being its signal completely supressed in the presence of an EG7-SAM. In an elegant approach, they demonstrated that this electron transfer inhibition is not due to a simple size or solubility driven permeation issue and recall the fact that the $[Fe(CN)_6]^{3-/4-}$ system is not an ideal outer-sphere redox couple. In contrast, they connect this behaviour to the impact of water molecules that play an important role in the change of the hydration shells of the oxidized and reduced form of this molecule, together with the reduced mobility of the water molecules in the EG7-SAM interface [42, 43].

Now, the electrical properties of SAMs involve not only electronic but also ionic modes of conduction. The ionic insulating properties of n-alkanethiol SAMs have been largely studied employing electrochemical impedance spectroscopy, in the absence of redox probes, as a way to test if the SAMs behave as an ideal parallel capacitor Helmholtz model either as a function of the applied potential or the medium chemical composition. In the present work, we have carried out impedance measurements as a function of the applied potential under the same experimental conditions of the experiments described in Figure 4 except that the redox probe was not present. The impedance spectra are represented as Bode phase plots to examine the values of the phase angle at low frequencies (c.a. 1 Hz) that is taken as a measure of the ideal capacitor system behaviour [44-46]. Figure 5a shows the variation of the phase angle values at 1 Hz with the applied potential for the EG7-SAM and for the naked gold electrodes. The CVs taken in the potential range of the

electrochemical profile for the gold electrode in this media for the naked and the EG7-SAM modified electrodes are also shown (Figure 5b). The CVs for the reductive and the oxidative desorption included are obtained by starting the scan at -0.15 V and scanning in the negative or positive directions, respectively, using two different freshly prepared EG7-SAMs to see the stability potential range. The double layer capacitance, C_{dl}, has been recorded under the same experimental conditions and the results are plotted together with the values obtained from the fitting of the impedance spectra taken as a function of potential (by using a RC circuit, where R is the solution resistance and C the capacitance and adding a parallel R element when necessary to account for the ionic resistance). The potential interval where the C_{dl} values are almost constant (~4.3±0.1 $\mu F/cm^2$) and is almost coincident with that of constant current in the CV. In this way, we can evaluate the potential range of film stability and compare it with the data of phase angle obtained. It is interesting to highlight that the phase angle approximately reaches the highest value of 90º, in a wide frequency range (see insert of Figure 5a) and that this behaviour is maintained in the potential interval that coincides with the stability of the film and with that where the ferricyanide probe is monitored (Figure 4). This behaviour agrees with results of EGn-SAMs studied by electrochemical impedance spectroscopy under somewhat different experimental conditions (0.1 M potassium phosphate + 0.2 M potassium chloride) that show that the EG chains contact with nearest neighbours leaving little room for nonhelical conformations or penetration of solvent and/or ions [17-19].

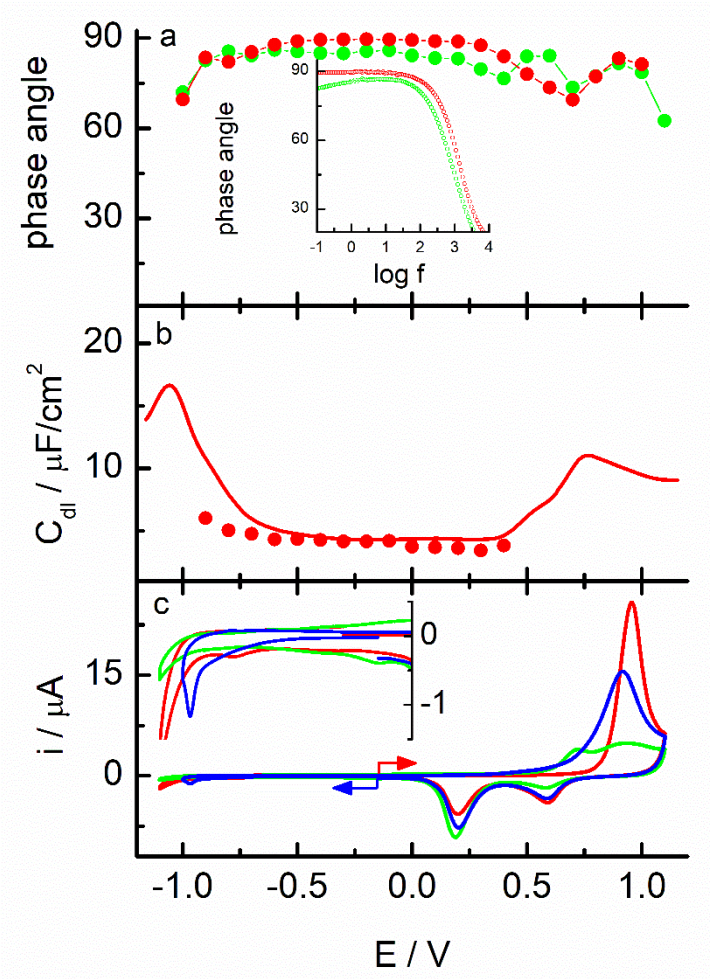

Figure 5. Insulating properties of the EG7-SAM gold electrode in KNO_3 0.1M. (a) Phase angles taken at the frequency of 1 Hz for the naked (solid green circle) and EG7-SAM (solid red circle) electrodes as a function of potential. Insert: Bode plots obtained at -0.1 V for the naked (green) and EG7-SAM (red) electrodes. (b) Double layer capacitance against potential recorded at a frequency of 500 Hz (solid red line) and capacitance values taken from the fitting of the impedance spectra (solid red circle). (c) CVs of the naked (green) and EG7-SAM gold electrodes recorded in the negative (blue) and positive (red) potential direction; scan rate: 0.02 V/s. Insert: enlarged view of the RD potential range.

These results together, allow us to conclude that the EG7-SAM have good blocking properties against electronic and ionic events in the potential range of SAM stability under neutral pH conditions.

3.3. Infrared characterization of EG7-SAMs

Infrared spectroscopy is one the most used techniques for the characterization of the EGn films and the assignation of the peaks for the different adopted structures of the chains within the SAMs is already well known [10, 17-21, 47-49]. One of the most addressed points has been the determination of the structural organization of the EGn chains in the films, as the helical conformation has been found to be less resistant to protein adsorption in comparison to the all-trans or disordered SAMs [17].

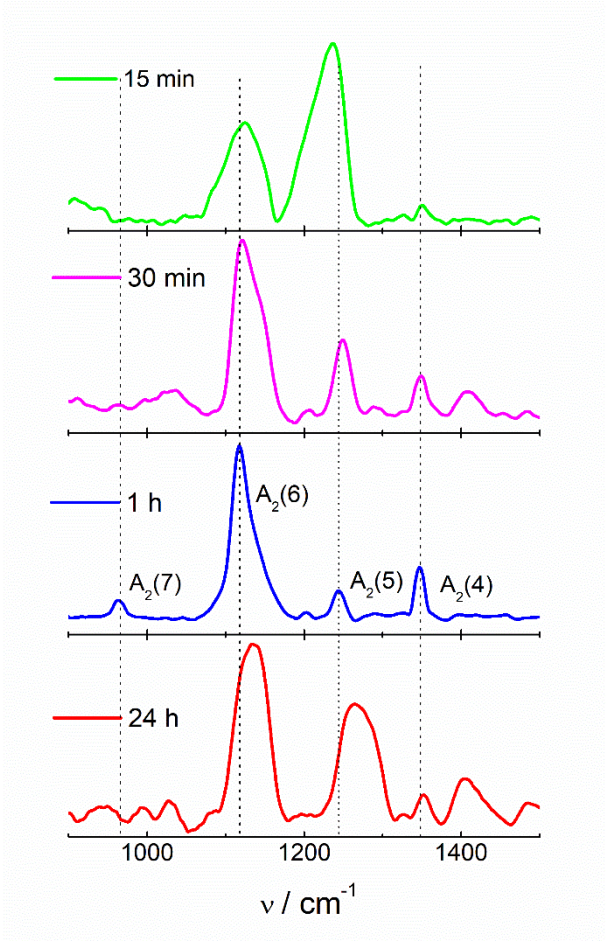

Figure 6. IRRAS spectra of the EG7-SAMs formed at different modification times on Au(111) single crystal surfaces recorded in the fingerprint region.

Figure 6 shows IRRAS of EG7-SAMs formed at different modification times on Au (111) single crystal surfaces. The fingerprint region has been used to prove the helical structure that it is characterized by the presence of a series of peaks at 1347, 1244, 1118 y 964 cm^{-1} which belong to vibration modes parallel to the helix axis (A_2(4) to (7)) for a 7/2 helical axis structure in a normal orientation to the substrate and the absence of signals at 1360, 1280, 1234, 1149, 1116, 1061, 947 y 843 cm^{-1}, related to vibration modes perpendicular to the chain axis (E_1(8) to (15)) [50]. As it can be observed in Figure 6, the EG7-SAM

formed in 15 min shows two broad signals at 1124 and 1237 cm^{-1}, and a well-defined but small peak at 1351 cm^{-1}. These broad peaks should contain more than one single component corresponding to different modes of chain organization within the layer, either parallel or perpendicular vibration modes. At a modification time of 30 min, the peaks become narrower and new peaks emerge, which match with the different vibration's modes of the EG chains in a helical conformation. Upon increasing modification time to 1 h, the typical spectrum for the 7/2 helical structure is obtained. However, at larger modification times, the typical fingerprint disappears indicating that the structure gets less ordered, as it can be inferred from the broadening of the peaks.

The signals obtained for the EG7-SAM prepared in 1 h coincide with these of the well-ordered helical structure described for H- and CH_3-terminated EGn-SAMs, in particular, asymmetric COC-stretching + CH_2-rocking, asymmetric COC-stretching, CH_2-twisting, CH_2-wagging and CH_2-bending vibrations at 965, 1119, 1243, 1347 and 1462 cm^{-1}, respectively [51, 52]. These findings agree with the electrochemical results that indicate that the optimum modification time for this EG7-SAM is of 1 h and indicate that the adopted conformation is the helical.

3.4. Contact Angle Measurements

Water contact angle measurements inform on the hydrophilic / hydrophobic character of the surfaces. We have measured the water contact angles of the EG7-SAMs formed at different modification times. The obtained values are gathered in Table 1. If the structure of the EG7 chain used in this study is considered, the contact angles must be sensitive to the organization of these molecules. Thus, the terminal methyl group, if exposed, will give a hydrophobic character to the layer in contrast to the possibility that they can be hidden in a disorganized structure. In fact, the EG7-SAM formed at 15 min shows a contact angle of 49 º that increases up to values higher than 60º for the SAMs formed at longer times. Although higher values have been measured for similar structures [17], the observed increase is an indication of the exposure of the methyl terminal groups to the external SAM face.

Table 1. Water contact angles of EG7-SAMs at different modification times (standard deviations ± 1º)

Modification time	EG7-SAM-Au / $\Theta_{(H2O)}$
0	67
15 min	49
30 min	59
1 h	64
24 h	63

3.5. XPS qualitative/quantitative characterization of t-OEG7

To get more insight into the composition of the EG7-SAM formed on a gold electrode, we have carried out XPS experiments. The spectra show peaks corresponding to S 2p, C 1s and O 1s that can be obtained in high resolution as shown in Figure 7. The S 2p spectrum is dominated by a strong peak at 162.0 eV that can be deconvoluted by two S $2p_{3/2,\ 1/2}$ doublets characteristics of thiolate species bound to gold (161.8 and 163.0 eV) and free thiol or di-sulphur groups (163.8 and 165.0 eV), the first one representing an area higher than 80 % of the overall signal. This fact points to the preferent adsorption of the EG7 molecules to the gold surface via S-Au bonds [10, 53-59]. The C 1s spectrum exhibits three components peaks at 284.6, 286.2 and 287.5 eV. The strongest peak at 286.2 eV is associated with the ether carbon atoms in the EG segments [60]. The O 1s spectrum also shows three components at 531.5, 532.6 and 533.7 eV. Similarly, the peak at 532.6 eV that represents the biggest contribution corresponds to the oxygen atoms in the EG segments.

The EG7-SAM characterized in this study is prepared from EG7 ethanol solutions. Thus, no water molecules are expected to be adsorbed in the SAM. However, ethanol molecules can be entrapped within the layer even after the just-prepared specimens are dried with a nitrogen stream. Thus, the extra peaks in the C 1s and O 1s signals can be due, on one side to molecules or fragments of ethanol [61] or to adventitious carbons coming from impurities within the SAMs.

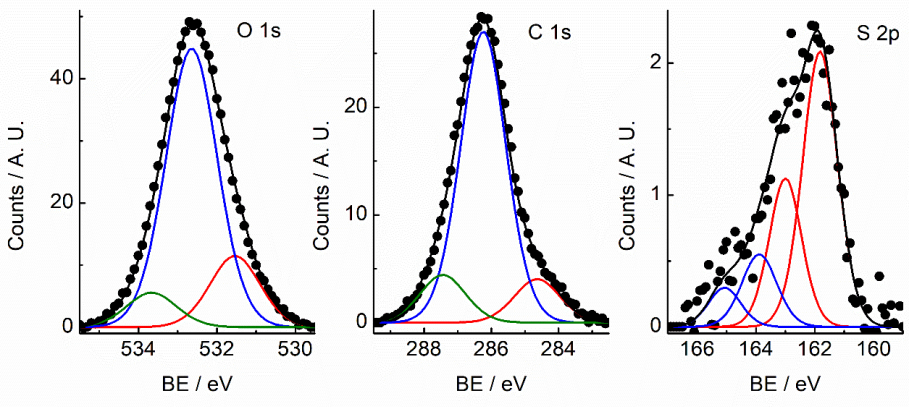

Figure 7. XPS spectra of the EG7-SAM gold electrode. The layer has been formed from an ethanolic solution in a modification time of 1 h. After modification, the modified substrate was dried with a nitrogen stream and subsequently maintained in a closed vial up to introduction in the vacuum XPS chamber.

3.6. Adsorption of bovine serum albumin (BSA) on the EG7-SAM.

To ascertain if the EG7-SAM formed on gold, under the experimental conditions described in this work, suffers unspecific adsorption of proteins, we have used the electrochemical quartz crystal microbalance to analyse the behaviour upon contacting with a solution of the protein bovine serum albumin (BSA). Figure 8 shows the CV curves for the RD process of the as-prepared EG7-SAM and that after contacting with a solution of 10 μM BSA for a long period of time (c.a., 2 hour), together with the frequency changes accompanying the electrochemical process.

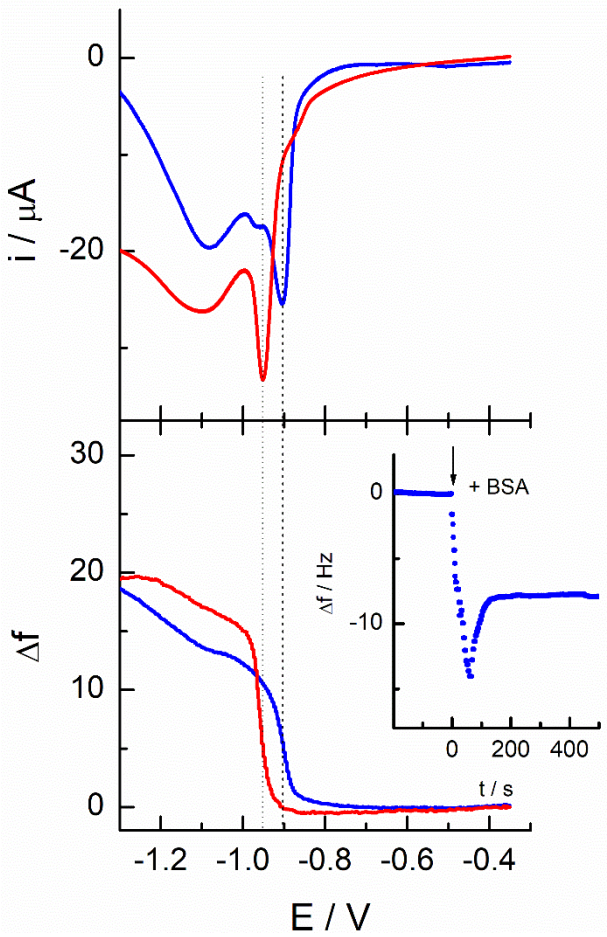

Figure 8. Electrochemical quartz crystal microbalance study of the RD process of an EG7-SAM on gold electrode, (red line) as-prepared and (blue line) after contacting with a BSA solution for 2 h. Insert: Changes in frequency of a EG7-SAM modified gold-quartz crystal upon introducing 10 μM BSA solution in sodium phosphate buffer at pH 7.4.

The mass change accompanying the complete release of an EG7-SAM is of around 40 ng, if the packing density of the EG7 molecules is taken as the fingerprint of 29 $Å^2$ per EG7 molecule determined above. The experimental mass change for the reductive desorption of the as-prepared SAM is of 29-30 ng. This value is close to the theoretical expected although, it cannot be ignored that this value can have some influences of the interfacial changes occurring simultaneously with the RD process. These processes include not only the replacement of the EG7 by water or electrolyte molecules [62] but also, the concomitant desorption of the water molecules co-adsorbed within the EG7-SAM [63]. The RD process is initiated after the frequency is equilibrated at the initial potential and as it can be observed, the value is kept constant up to the values where the desorption starts. At this point, coinciding with the voltammetric desorption peak, an

abrupt increase in frequency, describing a sigmoidal shape, is observed. At lower potentials, the frequency slightly increases up to reaching a plateau. The traces obtained for the desorption of the EG7-SAM after being exposed to the protein BSA shows a similar shape with a total frequency change that equals this of the as-prepared SAM. The only found difference is that the RD takes place at around 50 mV higher potential. This is indicative of a decrease in the stability of the layer during the exposure to the protein solution, probably due to the interaction of some protein molecules that, in some way, disturbs the compactness of the layer. Moreover, the equivalence in the mass changes that accompany the desorption is an indication of the absence of adsorbed protein on the EG7-SAM. The insert of Figure 8 shows the frequency trace obtained when, after the SAM is equilibrated with a phosphate saline solution at pH 7.4, the BSA protein is added to this solution. At this point (marked with the arrow in Figure 8), the frequency suddenly decreases and after 1 min, starts increasing up to reach a constant value. The total frequency decrease accounts for a mass increase of 11-12 ng that supposes less than 10% of a BSA monolayer. Taking together this small value and the fact that this excess of mass is not monitored in the RD of the EG7-SAM, we think that the protein molecules are weakly adsorbed, if it does, and get released when the substrate is contacted with the solution used to carry out the RD process [17].

4. Conclusions.

The EG7-SAM formed on a gold electrode from an ethanolic solution reaches a helical conformation at a modification time of 1 h. At longer times, the layer seems to acquire some disorganization, probably by the introduction of solvent molecules in the film structure. RD, IRRAS and contact angle measurements agree with this observation. While the RD shows well defined peaks that could be ascribed to ordered domains localized in different facets of the poly-oriented gold electrode, the IRRAS spectra taken in the fingerprint region show that the films prepared at modification times within 30 min and 1 h have the characteristic peaks of a helical conformation. The disorder obtained at longer times is, however, not translated to the contact angle values that keep constant under these conditions indicating that the disorganization of the helical conformation does not affect the terminal face of the film.

The compactness of the EG7-SAM is lower than that found in the EGn-alkanethiol terminated SAMs that show a fingerprint closer to these of the pure alkanethiol, probably

forced by the presence of the long alkane chain that acts as an arm anchoring to the gold surface. However, the EG7-SAM formed in the present work exhibits good blocking properties against the ferrocyanide redox probe as well as good ionic insulating properties in neutral aqueous saline solutions.

Finally, the EG7-SAM prepared from ethanol solution with 1 h of immersion time resists the adsorption of the BSA protein as monitored by the quartz crystal microbalance. The mass change obtained after 2 h of contact with the BSA solution corresponds to less than 10 % of a BSA monolayer. However, when the protein solution is removed, the few adsorbed proteins are released, as it is demonstrated in the mass changes accompanying the RD process of the EG7-SAM recorded for a pristine and a SAM substrate submitted to protein adsorption. This is a confirmation of the weak strength of the protein adsorption phenomena in the EG7-SAM obtained under these experimental conditions.

Acknowledgments. We thank the Ministerio de Ciencia e Innovación (Project RED2018-102412-T Network of Excellence Electrochemical Sensors and Biosensors), Junta de Andalucía and Universidad de Cordoba (UCO-FEDER-2018: ref. 1265074-2B and Plan Propio, Submod. 1.2. P.P. 2019) for financial support of this work. M.C. acknowledges Ministerio de Universidades for FPU 17/03873 grant.

5. Bibliography

[1] A. Abuchowski, J.R. McCoy, N.C. Palczuk, T. van Es, F.F. Davis, Effect of covalent attachment of polyethylene glycol on immunogenicity and circulating life of bovine liver catalase, J. Biol. Chem. 252(11) (1977) 3582-3586.

[2] L. Kong, F. Campbell, A. Kros, DePEGylation strategies to increase cancer nanomedicine efficacy, Nanoscale Horiz. 4(2) (2019) 378-387.

[3] Z. Hussain, S. Khan, M. Imran, M. Sohail, S.W.A. Shah, M. de Matas, PEGylation: a promising strategy to overcome challenges to cancer-targeted nanomedicines: a review of challenges to clinical transition and promising resolution, Drug Deliv. Transl. Res. 9(3) (2019) 721-734.

[4] J.S. Suk, Q. Xu, N. Kim, J. Hanes, L.M. Ensign, PEGylation as a strategy for improving nanoparticle-based drug and gene delivery, Adv. Drug Deliver. Rev. 99 (2016) 28-51.

[5] J.V. Jokerst, T. Lobovkina, R.N. Zare, S.S. Gambhir, Nanoparticle PEGylation for imaging and therapy, Nanomedicine 6(4) (2011) 715-728.

[6] M. Tanaka, T. Sawaguchi, Y. Hirata, O. Niwa, K. Tawa, C. Sasakawa, K. Kuraoka, Properties of modified surface for biosensing interface, J. Colloid Inter. Sci. 497 (2017) 309-316.
[7] R. Ortiz, S. Olsen, E. Thormann, Salt-Induced Control of the Grafting Density in Poly(ethylene glycol) Brush Layers by a Grafting-to Approach, Langmuir 34(15) (2018) 4455-4464.
[8] K.L. Prime, G.M. Whitesides, Adsorption of Proteins onto Surfaces Containing End-Attached Oligo(Ethylene Oxide) - A Model System Using Self-Assembled Monolayers, J. Am. Chem. Soc. 115(23) (1993) 10714-10721.
[9] S. Herrwerth, W. Eck, S. Reinhardt, M. Grunze, Factors that determine the protein resistance of oligoether self-assembled monolayers - Internal hydrophilicity, terminal hydrophilicity, and lateral packing density, J. Am. Chem. Soc. 125(31) (2003) 9359-9366.
[10] P. Harder, M. Grunze, R. Dahint, G.M. Whitesides, P.E. Laibinis, Molecular conformation in oligo(ethylene glycol)-terminated self-assembled monolayers on gold and silver surfaces determines their ability to resist protein adsorption, J. Phys. Chem. B 102(2) (1998) 426-436.
[11] M.W.A. Skoda, F. Schreiber, R.A.J. Jacobs, J.R.P. Webster, M. Wolff, R. Dahint, D. Schwendel, M. Grunze, Protein Density Profile at the Interface of Water with Oligo(ethylene glycol) Self-Assembled Monolayers, Langmuir 25(7) (2009) 4056-4064.
[12] S.I. Jeon, J.H. Lee, J.D. Andrade, P.G. Degennes, Protein Surface Interactions in the Presence of Polyethylene Oxide. 1. Simplified Theory, J. Colloid Inter. Sci. 142(1) (1991) 149-158.
[13] K. Feldman, G. Hahner, N.D. Spencer, P. Harder, M. Grunze, Probing resistance to protein adsorption of oligo(ethylene glycol)-terminated self-assembled monolayers by scanning force microscopy, J. Am. Chem. Soc. 121(43) (1999) 10134-10141.
[14] R.L.C. Wang, H.J. Kreuzer, M. Grunze, Molecular conformation and solvation of oligo(ethylene glycol)-terminated self-assembled monolayers and their resistance to protein adsorption, J. Phys. Chem. B 101(47) (1997) 9767-9773.
[15] D.J. Vanderah, C.W. Meuse, V. Silin, A.L. Plant, Synthesis and Characterization of Self-Assembled Monolayers of Alkylated 1-Thiahexa(ethylene oxide) Compounds on Gold, Langmuir 14(24) (1998) 6916-6923.
[16] D.J. Vanderah, C.P. Pham, S.K. Springer, V. Silin, C.W. Meuse, Characterization of a series of self-assembled monolayers of alkylated 1-thiaoligo (ethylene oxides)(4-8) on Gold, Langmuir 16(16) (2000) 6527-6532.

[17] D.J. Vanderah, G. Valincius, C.W. Meuse, Self-assembled monolayers of methyl 1-thiahexa(ethylene oxide) for the inhibition of protein adsorption, Langmuir 18(12) (2002) 4674-4680.

[18] D.J. Vanderah, J. Arsenault, H. La, R.S. Gates, V. Silin, C.W. Meuse, G. Valincius, Structural variations and ordering conditions for the self-assembled monolayers of HS(CH2CH2O)(3-6)CH3, Langmuir 19(9) (2003) 3752-3756.

[19] D.J. Vanderah, T. Parr, V. Silin, C.W. Meuse, R.S. Gates, H. La, G. Valincius, Isostructural Self-Assembled Monolayers. 2. Methyl 1-(3-Mercaptopropyl)-oligo(ethylene oxide)s, Langmuir 20(4) (2004) 1311-1316.

[20] L. Malysheva, A. Onipko, R. Valiokas, B. Liedberg, First-Principle DFT and MP2 Modeling of Infrared Reflection−Absorption Spectra of Oriented Helical Ethylene Glycol Oligomers, J. Phys. Chem. B 109(27) (2005) 13221-13227.

[21] L. Malysheva, A. Onipko, T. Fyrner, H.-H. Lee, R.n. Valiokas, P. Konradsson, B. Liedberg, Spectroscopic Characterization and Modeling of Methyl- and Hydrogen-Terminated Oligo(ethylene glycol) Self-Assembled Monolayers, J. Phys. Chem. C 116(22) (2012) 12008-12016.

[22] R. Schlapak, D. Caruana, D. Armitage, S. Howorka, Semipermeable poly(ethylene glycol) films: the relationship between permeability and molecular structure of polymer chains, Soft Matter 5(21) (2009) 4104-4112.

[23] C.E. Hotchen, I.J. Maybury, G.W. Nelson, J.S. Foord, P. Holdway, F. Marken, Amplified electron transfer at poly-ethylene-glycol (PEG) grafted electrodes, Phys. Chem. Chem. Phys. 17(17) (2015) 11260-11268.

[24] K. Nekoueian, C.E. Hotchen, M. Amiri, M. Sillanpää, G.W. Nelson, J.S. Foord, P. Holdway, A. Buchard, S.C. Parker, F. Marken, Interfacial Electron-Shuttling Processes across KolliphorEL Monolayer Grafted Electrodes, ACS Appl. Mater. Interfaces 7(28) (2015) 15458-15465.

[25] T. Doneux, L. Yahia Cherif, C. Buess-Herman, Controlled Tuning of the Ferri/Ferrocyanide Electron Transfer at Oligo(Ethylene Glycol)-Modified Electrodes, Electrochim. Acta 219 (2016) 412-417.

[26] T. Doneux, A. de Ghellinck, E. Triffaux, N. Brouette, M. Sferrazza, C. Buess-Herman, Electron Transfer Across an Antifouling Mercapto-hepta(ethylene glycol) Self-Assembled Monolayer, J. Phys. Chem. C 120(29) (2016) 15915-15922.

[27] N. Gu, L. Niu, S. Dong, Simultaneous determination of both the calibration constant in an electrochemical quartz crystal microbalance and the active surface area of a polycrystalline gold electrode, Electrochem. Commun. 2(1) (2000) 48-50.
[28] R. Madueno, J.M. Sevilla, T. Pineda, A.J. Roman, M. Blazquez, A voltammetric study of 6-mercaptopurine monolayers on polycrystalline gold electrodes, J. Electroanal. Chem. 506(2) (2001) 92-98.
[29] D.F. Yang, C.P. Wilde, M. Morin, Electrochemical desorption and adsorption of nonyl mercaptan at gold single crystal electrode surfaces, Langmuir 12(26) (1996) 6570-6577.
[30] S. Yoshimoto, T. Sawaguchi, F. Mizutani, I. Taniguchi, STM and voltammetric studies on the structure of a 4-pyridinethiolate monolayer chemisorbed on Au(100)-(1×1) surface, Electrochem. Commun. 2(1) (2000) 39-43.
[31] K. Arihara, T. Ariga, N. Takashima, T. Okajima, F. Kitamura, K. Tokuda, T. Ohsaka, Multiple voltammetric waves for reductive desorption of cysteine and 4-mercaptobenzoic acid monolayers self-assembled on gold substrates, Phys. Chem. Chem. Phys. 5(17) (2003) 3758-3761.
[32] T. Doneux, M. Steichen, A. De Rache, C. Buess-Herman, Influence of the crystallographic orientation on the reductive desorption of self-assembled monolayers on gold electrodes, J. Electroanal. Chem. 649(1-2) (2010) 164-170.
[33] S.S. Wong, M.D. Porter, Origin of the multiple voltammetric desorption waves of long-chain alkanethiolate monolayers chemisorbed on annealed gold electrodes, J. Electroanal. Chem. 485(2) (2000) 135-143.
[34] D.M. Kolb, J. Schneider, Surface Reconstruction in Electrochemistry - Au(100)-(5x20), Au(111)-(1x23) and Au(110)-(1x2), Electrochim. Acta 31(8) (1986) 929-936.
[35] P. Ramirez, R. Andreu, A. Cuesta, C.J. Calzado, J.J. Calvente, Determination of the potential of zero charge of Au(111) modified with thiol monolayers, Anal. Chem. 79(17) (2007) 6473-6479.
[36] R.C. Salvarezza, P. Carro, The electrochemical stability of thiols on gold surfaces, J. Electroanal. Chem. 819 (2018) 234-239.
[37] C.A. Widrig, C. Chung, M.D. Porter, The electrochemical desorption of n-alkanethiol monolayers from polycrystalline gold and silver electrodes, J. Electroanal. Chem. 310(1-2) (1991) 335-59.
[38] O. Azzaroni, M.E. Vela, G. Andreasen, P. Carro, R.C. Salvarezza, Electrodesorption Potentials of Self-Assembled Alkanethiolate Monolayers on Ag(111) and Au(111). An

Electrochemical, Scanning Tunneling Microscopy and Density Functional Theory Study, J. Phys. Chem. B 106(47) (2002) 12267-12273.
[39] T. Laredo, J. Leitch, M. Chen, I.J. Burgess, J.R. Dutcher, J. Lipkowski, Measurement of the Charge Number Per Adsorbed Molecule and Packing Densities of Self-Assembled Long-Chain Monolayers of Thiols, Langmuir 23(11) (2007) 6205-6211.
[40] M. Baghbanzadeh, C.M. Bowers, D. Rappoport, T. Żaba, L. Yuan, K. Kang, K.-C. Liao, M. Gonidec, P. Rothemund, P. Cyganik, A. Aspuru-Guzik, G.M. Whitesides, Anomalously Rapid Tunneling: Charge Transport across Self-Assembled Monolayers of Oligo(ethylene glycol), J. Am. Chem. Soc. 139(22) (2017) 7624-7631.
[41] D. Garcia-Raya, R. Madueno, J. Manuel Sevilla, M. Blazquez, T. Pineda, Electrochemical characterization of a 1,8-octanedithiol self-assembled monolayer (ODT-SAM) on a Au(111) single crystal electrode, Electrochim. Acta 53(27) (2008) 8026-8033.
[42] C. Dicke, G. Hähner, pH-Dependent Force Spectroscopy of Tri(ethylene Glycol)- and Methyl-Terminated Self-Assembled Monolayers Adsorbed on Gold, J. Am. Chem. Soc. 124(42) (2002) 12619-12625.
[43] H.I. Kim, J.G. Kushmerick, J.E. Houston, B.C. Bunker, Viscous “Interphase” Water Adjacent to Oligo(ethylene glycol)-Terminated Monolayers, Langmuir 19(22) (2003) 9271-9275.
[44] E. Boubour, R.B. Lennox, Insulating Properties of Self-Assembled Monolayers Monitored by Impedance Spectroscopy, Langmuir 16(9) (2000) 4222-4228.
[45] E. Boubour, R.B. Lennox, Potential-Induced Defects in n-Alkanethiol Self-Assembled Monolayers Monitored by Impedance Spectroscopy, J. Phys. Chem. B 104(38) (2000) 9004-9010.
[46] E. Boubour, R.B. Lennox, Stability of ω-Functionalized Self-Assembled Monolayers as a Function of Applied Potential, Langmuir 16(19) (2000) 7464-7470.
[47] H.-H. Lee, Z. Ruzele, L. Malysheva, A. Onipko, A. Gutes, F. Bjorefors, R. Valiokas, B. Liedberg, Long-Chain Alkylthiol Assemblies Containing Buried In-Plane Stabilizing Architectures, Langmuir 25(24) (2009) 13959-13971.
[48] R. Valiokas, L. Malysheva, A. Onipko, H.H. Lee, Z. Ruzele, S. Svedhem, S.C.T. Svensson, U. Gelius, B. Liedberg, On the quality and structural characteristics of oligo(ethylene glycol) assemblies on gold: An experimental and theoretical study, J. Electron Spectros. Relat. Phenomena 172(1-3) (2009) 9-20.

[49] L. Malysheva, A. Onipko, B. Liedberg, Ab Initio Modeling of Defect Signatures in Infrared Reflection−Absorption Spectra of SAMs Exposing Methyl- and Hydrogen-Terminated Oligo(ethylene glycols), J. Phys. Chem. A 112(4) (2008) 728-736.
[50] M. Kobayashi, M. Sakashita, Morphology Dependent Anomalous Frequency-Shifts of Infrared-Absorption Bands of Polymer Crystals - Interpretation in Terms of Transition Dipole -Dipole Coupling Theory, J. Chem. Phys. 96(1) (1992) 748-760.
[51] T. Miyazawa, Y. Ideguchi, K. Fukushima, Molecular Vibrations and Structure of High Polymers. 3. Polarized Infrared Spectra, Normal Vibrations and Helical Conformation of Polyethylene Glycol, J. Chem. Phys. 37(12) (1962) 2764-2776.
[52] T. Yoshihara, S. Murahashi, H. Tadokoro, Normal Vibrations of Polymer Molecules of Helical Conformation. 4. Polyethylene Oxide + Polyethylene-D4 Oxide, J. Chem. Phys. 41(9) (1964) 2902-2911.
[53] Y.L. Jeyachandran, T. Weber, A. Terfort, M. Zharnikov, Application of Long Wavelength Ultraviolet Radiation for Modification and Patterning of Protein-Repelling Monolayers, J. Phys. Chem. C 117(11) (2013) 5824-5830.
[54] D.G. Castner, K. Hinds, D.W. Grainger, X-ray photoelectron spectroscopy sulfur 2p study of organic thiol and disulfide binding interactions with gold surfaces, Langmuir 12(21) (1996) 5083-5086.
[55] M.M. Walczak, C.A. Alves, B.D. Lamp, M.D. Porter, Electrochemical and X-ray photoelectron spectroscopic evidence for differences in the binding sites of alkanethiolate monolayers chemisorbed at gold, J. Electroanal. Chem. 396(1-2) (1995) 103-114.
[56] F. Schreiber, Structure and growth of self-assembling monolayers, Prog. Surf. Sci. 65(5-8) (2000) 151-256.
[57] C.D. Bain, E.B. Troughton, Y.T. Tao, J. Evall, G.M. Whitesides, R.G. Nuzzo, Formation of Monolayer Films by the Spontaneous Assembly of Organic Thiols from Solution onto Gold, J. Am. Chem. Soc. 111(1) (1989) 321-335.
[58] R.G. Nuzzo, B.R. Zegarski, L.H. Dubois, Fundamental-Studies of the Chemisorption of Organosulfur Compounds on Au(111) - Implications for Molecular Self-Assembly on Gold Surfaces, J. Am. Chem. Soc. 109(3) (1987) 733-740.
[59] H. Rieley, G.K. Kendall, F.W. Zemicael, T.L. Smith, S. Yang, X-ray Studies of Self-Assembled Monolayers on Coinage Metals. 1. Alignment and Photooxidation in 1,8-Octanedithiol and 1-Octanethiol on Au, Langmuir 14(18) (1998) 5147-5153.
[60] C. Palegrosdemange, E.S. Simon, K.L. Prime, G.M. Whitesides, Formation of Self-Assembled Monolayers by Chemisorption of Derivatives of Oligo(Ethylene Glycol) of

Struture HS(CH2)11(OCH2CH2)META-OH on Gold, J. Am. Chem. Soc. 113(1) (1991) 12-20.
[61] Z. Liu, T. Duchoň, H. Wang, D.C. Grinter, I. Waluyo, J. Zhou, Q. Liu, B. Jeong, E.J. Crumlin, V. Matolín, D.J. Stacchiola, J.A. Rodriguez, S.D. Senanayake, Ambient pressure XPS and IRRAS investigation of ethanol steam reforming on Ni–CeO2(111) catalysts: an in situ study of C–C and O–H bond scission, Phys. Chem. Chem. Phys. 18(25) (2016) 16621-16628.
[62] T. Kawaguchi, H. Yasuda, K. Shimazu, M.D. Porter, Electrochemical Quartz Crystal Microbalance Investigation of the Reductive Desorption of Self-Assembled Monolayers of Alkanethiols and Mercaptoalkanoic Acids on Au, Langmuir 16(25) (2000) 9830-9840.
[63] M. Yoshimoto, K. Honda, S. Kurosawa, M. Tanaka, Dynamic Properties of Self-Assembled Monolayers of Mercapto Oligo(ethylene oxide) Methyl Ether on an Oscillating Solid–Liquid Interface, J. Phys. Chem. C 118(29) (2014) 16067-16073.